Title

Decoding the neural dynamics of oculomotor decision making in humans

Authors

Thomas Thiery[1], Anne-Lise Saive[1], Etienne Combrisson[1,2], Arthur Dehgan[1], Julien Bastin[3], Philippe Kahane[3], Alain Berthoz[4], Jean-Philippe Lachaux[2], Karim Jerbi[1]

Affiliations

[1] Cognitive & Computational Neuroscience Lab, Psychology Department, University of Montreal, QC, Canada

[2] Centre de Recherche en Neurosciences de Lyon (CRNL), Lyon, France

[3] Grenoble Institut des Neurosciences, Grenoble, France

[4] Collège de France, Paris, France

Highlights

- First LFP recordings in humans performing an oculomotor decision-making task
- Free-choice saccade trials exhibit sustained frontoparietal high gamma activity
- Machine learning analytics unravel underlying spectral and temporal brain dynamics
- Single-trial saccade-locked gamma distinguish planning and execution processes

Summary

Freely choosing an action between alternatives activates a widely distributed decision circuit in the brain. Primate studies suggest that oculomotor decision processes are encoded by high-frequency components of local field potentials (LFPs) recorded in frontal and parietal areas. To what extent these LFP observations extend to oculomotor decision-making in humans is unknown. Here, we address this question using intracerebral EEG recordings from 778 sites across six surgical epilepsy patients. Free saccade choices were associated with sustained high gamma (60-140 Hz) activity during the delay period in prefrontal and parietal areas. Importantly, employing single-trial signal classification to contrast free, instructed and control trials, we were able to isolate decision-related activity from sensory and motor processes. Our findings provide the first direct electrophysiological evidence in humans for the role of high gamma activity in parietal and prefrontal areas in the intrinsically driven process of choosing among competing behavioral alternatives during free choice.

Introduction

Deciding where to look to explore the visual world, i.e. picking one out of many alternative targets is a crucial aspect of our daily interactions with the environment. Exploring the neural mechanisms underlying eye movement control provides a promising approach for learning about sensorimotor and cognitive aspects of voluntary action selection and planning (Sweeney et al., 2007). According to neurophysiological accounts of motor decision-making, movement selection appears to be simultaneously represented in a collection of parietal and frontal areas (e.g., Basso and Wurtz, 1998; Cisek and Kalaska, 2010; Platt and Glimcher, 1999; Shadlen and Newsome, 2001). Unit recordings as well as local field potentials (LFPs) in animals performing delayed-response tasks show persistent neuronal activity in prefrontal (Brody et al., 2003; Goard et al.; Kim and Shadlen, 1999; Rainer et al., 1999; Riley and Constantinidis, 2015; Siegel et al., 2015; Stokes, 2015) and parietal (Chafee and Goldman-Rakic, 1998; Huang et al, 2013.; Pesaran et al., 2002; Romo and de Lafuente, 2013) areas during decision-making, working memory and response selection processes, including free choice oculomotor tasks (Platt and Glimcher, 1999). Specifically, eye movement decisions appear to involve the same effector specific circuits that execute eye movements, which include the lateral intraparietal area (LIP) (Dorris and Glimcher, 2004; Gold and Shadlen, 2007; Platt and Glimcher, 1999; Sugrue et al., 2004; Yang and Shadlen, 2007), and the frontal eye fields (FEF) (Coe et al., 2002; Schall and Bichot, 1998) in non-human primates.

In humans, converging evidence from neuroimaging studies suggests that the neural processes which mediate saccade decisions, planning and execution arise across large-scale brain networks that involve parietal, frontal, and motor cortices (Anderson et al., 2012; Kagan et al., 2010; McDowell et al., 2008; Sweeney et al., 2007). A parietal oculomotor field (PEF), located in the posterior part of the parietal cortex (which is thought to correspond to LIP in monkeys) (Berman et al. 1999), seems to be principally implicated in triggering reflex saccades. By contrast, the FEF is thought to play a central role in preparation of the saccades by coding both the motor preparation and the intention to make a saccade (Bastin et al., 2012; Blanke and Seeck, 2003; Connolly et al., 2002; Olk et al., 2006; Petit et al., 1997; Pierrot-Deseilligny et al., 2002; Tobler and Müri, 2002). Lastly, two functional magnetic resonance imaging (fMRI) studies using a delayed saccade task have specifically shown that voluntary saccades were preceded by activation in the dorsolateral prefrontal cortex (DLPFC) and in the frontal eye fields, suggesting the involvement of these areas in the process of choosing where to look when facing two possible visual targets (Khonsari et al., 2007; Milea et al., 2007). However, fMRI can unfortunately not resolve the precise

temporal dynamics of activity in these brain areas, neither can it probe the role of rhythmic brain activity. To address these questions in humans, electrophysiological investigations are required.

Non-invasive electrophysiological studies have demonstrated the involvement of high-frequency neuronal oscillations in several areas ("eye or oculomotor fields") of the cerebral cortex during saccade planning and execution using techniques such as MEG (Carl et al., 2016; Jerbi et al., 2008; Moon et al., 2007; Van Der Werf et al., 2009; Werf et al., 2008, 2010) and EEG (Forgacs et al., 2008; Park et al., 2014). Despite being extremely insightful, non-invasive techniques have several limitations in terms of signal quality, spatial resolution and sensitivity to artefacts. Fortunately, it is possible in some rare cases to access invasive electrophysiological recordings in humans (e.g. surgical epilepsy patients) and thus probe task-based changes via direct LFP recordings. The latter reflect the synchronized postsynaptic potentials of local populations of neurons (Frost and Pöppel, 1976; Mitzdorf, 1985) and allow for direct comparisons between invasive recordings of population-level activity in human and non-human primates. A handful of studies have benefited from direct recordings of neural activity (e.g. in human FEF and DLPFC) to probe neural activation in the frontal eye fields during saccade execution (peri-saccade activity) in humans using intracranial EEG (Lachaux et al., 2006a; Sakamoto et al., 1991; Yamamoto et al., 2004). Importantly, Lachaux and colleagues (2006a) found that the preparation and the generation of saccades were subserved by focal and transient increases of EEG HG activity (above 60 Hz) in the FEF. To our knowledge, no study has so far investigated the neural correlates of oculomotor decisions (i.e. free choice saccades) using direct intracranial recordings in humans.

Taken together, previous findings from oculomotor and decision-making studies in non-human primates provide converging evidence for the central role of high-frequency LFP components in eye movement selection and execution. Although, some evidence from non-invasive studies partly support these observations in humans, direct electrophysiological measurements are necessary to bridge the gap between human and non-human primate literature on oculomotor decision-making. In the present study, we probe for the first time the temporal, spectral and spatial characteristics of human cortical networks engaged in the selection, planning and execution of saccades with unprecedented resolution thanks to multi-site intracerebral EEG (iEEG) recordings. In particular, we set out to test the predictions that (i) the temporal dynamics of delay-period LFP would differ between *instructed* and *self-chosen* saccade trials, and that (ii) the most prominent differences will be visible in high-frequency LFP components in key frontal and parietal areas. In brief, we found that the intrinsically driven process of selecting among competing behavioral alternatives during free-choice decisions is associated with sustained increases of high gamma (HG) (60-140 Hz) activity in distinct frontal and parietal areas. By

contrast, planning instructed saccades was associated with short-lived transient HG increases in fronto-parietal brain regions alongside a suppression of beta oscillations (16-25 Hz) mainly in motor-related areas. Furthermore, by contrasting free and instructed saccade conditions with a control condition where no directional information was available during the delay period, we were able to isolate decision-related HG activity from purely sensory, visuomotor transformation and planning processes, as well as from purely oculomotor execution activity.

Results

Six subjects (6 females, mean age 30.3 ± 9.6, see STAR Methods and Figure 1B, C) performed a delayed saccade task (Figure 1A) while electrophysiological data were recorded from multi-lead EEG depth electrodes. In each trial, participants were instructed to perform horizontal saccades toward one of two targets, but only after a variable delay period. The information about saccade direction was indicated by a visually presented central cue (Cue 1), followed by a saccade execution Go signal (Cue 2). The task consisted of three interleaved experimental conditions (Figure 1A): In the ***Free*** condition, a diamond at Cue 1 prompted the participants to freely choose the direction of the forthcoming saccade. In the ***Instructed*** condition, an arrow pointing left or right indicated to the participants the direction of the saccade they were to prepare. After a variable delay (3.5-10.5 seconds) during which the participants prepared the adequate saccade while fixating the central fixation point, a GO signal (Cue 2) prompted the participants to immediately execute the saccade. In the ***Control*** condition, participants were presented with a square at Cue 1, indicating that they would need to wait for the GO signal (Cue 2) to find out the required saccade direction and execute it immediately. Behavioral saccade onset latency data were collected and spectral power features were extracted from the iEEG data across multiple time windows and all electrode sites. Power features were computed in five standard frequency bands: theta (θ) [4–8 Hz], alpha (α) [8–15 Hz], beta (β) [16–30 Hz], low-gamma (low γ) [30–60] and high gamma (high γ, HG) [60-140 Hz]). A supervised machine learning framework was implemented to decode (through space, time and frequency) the experimental conditions (free, instructed and control), and thereby identify the most discriminant neural patterns that distinguish between free-choice and instructed actions during saccade planning and execution (see STAR Methods for details).

Behavioral results

We computed the mean reaction times (RTs, i.e., saccade onset latency) for each of our experimental conditions across all patients, and found that mean RTs were significantly longer during the ***Control*** (*mean RT = 438 ms)* condition compared to both ***Free*** ($mean\ RT = 380\ ms$, $p < 0.001$) and ***Instructed*** ($mean\ RT = 339\ ms, p < 0.001$) conditions (see Figure 1D). No significant differences were found when we compared reaction times between ***Free*** and ***Instructed*** conditions $p = 0.48$).These results are consistent with the fact that the availability of saccade target information (whether self-generated or instructed) during the delay period allowed the participants to plan the upcoming saccades, and execute them faster upon the Go signal compared to the ***Control*** condition where no directional information was available during the delay period. Mean saccade duration, saccade speed, mean latency and the number of saccades executed per condition by each patient are reported in Table S1.

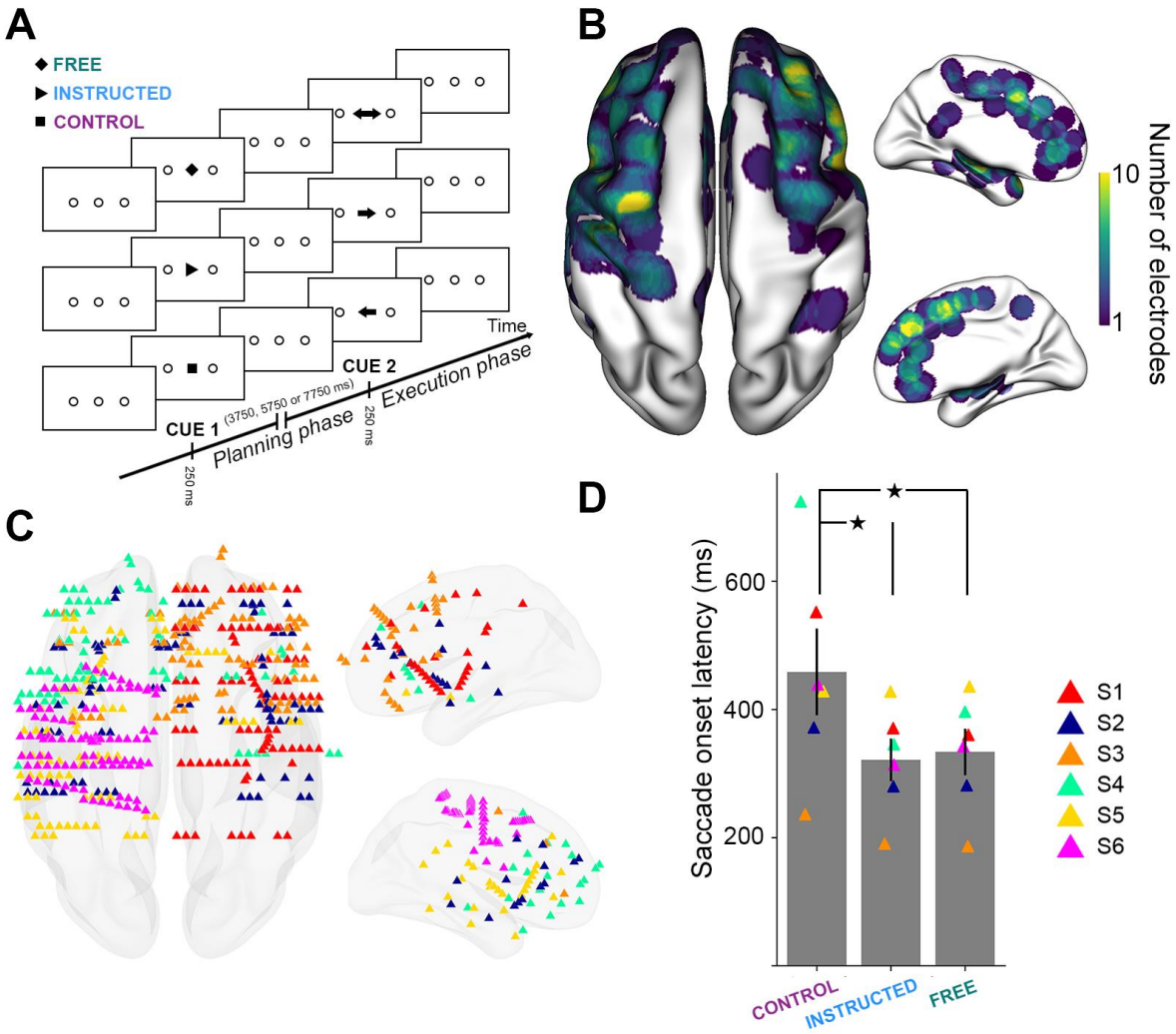

Figure 1. Experimental design and distribution of intracranial electrode contacts across subjects. A. Experimental design of the delayed motor task. For each trial, participants were instructed to perform horizontal saccades toward one of two targets after a delay of 3750 ms, 5750 ms or 7750 ms, depending on a visually presented central cue appearing briefly for 250 ms. **B.** Top, left and right view of the depth-electrode recording sites, projected on a standard 3D MNI brain. Left: Rostral is up, Right: medial views. **C.** Top, left and right views of the number of recording sites that contribute to each vertex (i.e. spatial density) projected on a standard 3D MNI brain. Electrodes contribute to a location when they are within 10 mm of a given site on the brain surface. In all brain images, right side of the image is the right side of the brain. **D.** Barplot of mean reaction times for the three conditions across all participants (***Control***, ***Instructed***, ***Free***). Each triangle represents the mean reaction times for one subject.

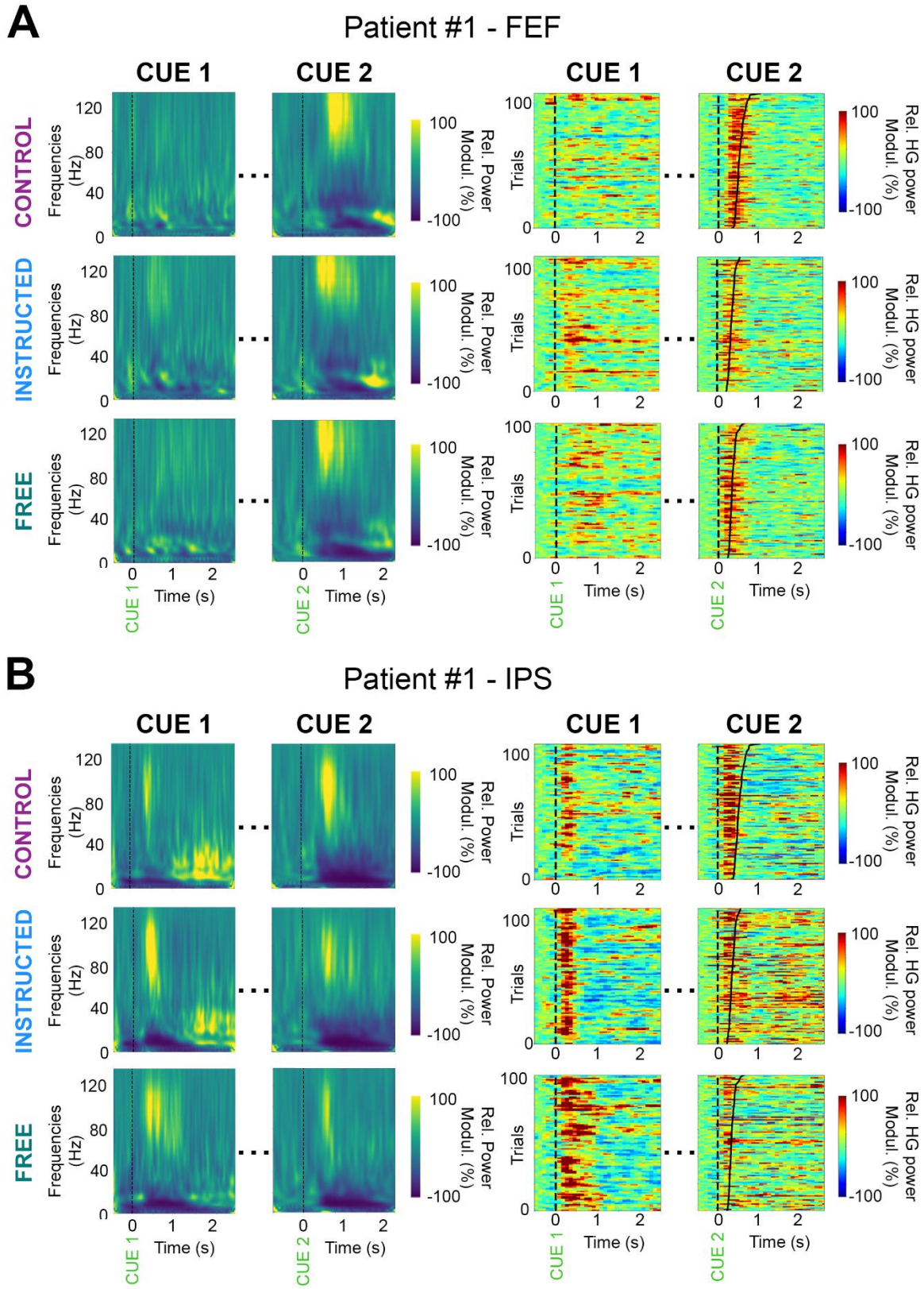

Figure 2. Illustrative time-frequency maps and single-trial high gamma (HG) activity in FEF and IPS. Time-frequency maps (left) and single-trial high gamma plots (right) from two recording sites in an illustrative patient. Data are shown for the three experimental conditions (*Control*, *Instructed* and *Free*), during planning (Cue 1, stimulus onset) and execution (Cue 2, go signal). Trials in the single-trial gamma plots are sorted according to saccade onset latencies. (IPS: intraparietal sulcus, FEF: Frontal Eye Field).

Temporal dynamics of brain activity during free versus instructed saccade planning

Figure 2 illustrates examples of time-frequency maps in FEF and IPS from two patients, as well as single-trial high-gamma activity, aligned to cue 1 and to cue 2. Interestingly, a prominent stimulus-locked burst is observed to both cues in IPS, but only to the second cue in FEF. To more quantitatively analyze task-based neural modulations during the delay period (and compare them across the ***free*** and ***instructed*** saccade conditions) we first searched for statistically significant time-resolved discrimination between iEEG spectral power measured during the delay-period (post-Cue 1) and baseline levels (pre-Cue1) using data-driven analytics (see STAR methods). By monitoring the success of standard cross-validated linear discriminant analysis (LDA) in distinguishing delay activity from pre-stimulus baseline, we identified relevant saccade decision/planning activity in LFP data from each subject. The supervised classification was conducted across space (all electrode sites), frequency bands (theta to high gamma) and a 2000 ms window after stimulus onset (successive 250ms time windows with an overlap of 100ms, see STAR methods). Figure 3 (A-C) shows that the frequency band with the highest mean decoding accuracies was the HG (60-140 Hz) band. Interestingly, for the classification of ***Free vs baseline*** the mean gamma decoding accuracy (DA) across all significant electrodes was 80.6 % (max DA = 92.6 %) while for ***Instructed vs baseline*** the mean gamma DA was 82.1 % (max DA = 98.7 %). In addition, HG was also the most prominent band in terms of number of sites with significant classification accuracies for these two classifications.

Next, we went on to characterize the temporal evolution of this HG activity during the delay period. To this end, we analyzed changes in spectral power of cue-aligned signals in consecutive non-overlapping time windows ranging from 500 ms before to 2000 ms after stimulus onset (Cue 1). Figures 3D and 3F show that significant decoding was predominantly distributed in a network of frontal and parietal areas during saccade planning for ***Free***, and ***Instructed*** conditions (6/6 subjects for both conditions, $p < 0.01$, see STAR methods). This parieto-frontal cortical network was very similar (high degree of spatial overlap) whether participants were freely deciding where to look or planning instructed saccades. Crucially, however, we found that HG activity in frontal areas such as FEF and DLPFC continues to differ from baseline in the ***free*** trials (Figure 3E) in later time windows (>1000 ms) whereas this is not the case in the ***instructed*** trials (Figure 3G). Moreover, evidence for a later task-specific HG modulation was also visible through cortical mapping of the latency of maximum decoding accuracies in free (Figure 3F) and instructed (Figure 3H) saccade conditions. For free saccade trials the peak of decoding (free vs baseline) occurred around 1500 ms after stimulus onset, substantially later than the maximum decoding peaks for instructed saccades.

Taken together, these discrepancies across conditions in the temporal evolution of prominent modulations during the delay-period suggests that decision-related frontal HG activity is more sustained and peaks later in time, in free compared to instructed saccades. In contrast, when no choice is involved (i.e. instructed condition), task-related information reflected in HG activity is more transient, and most relevant (i.e. peak decoding) shortly after stimulus onset in a widespread parieto-frontal network (Figure 3G).

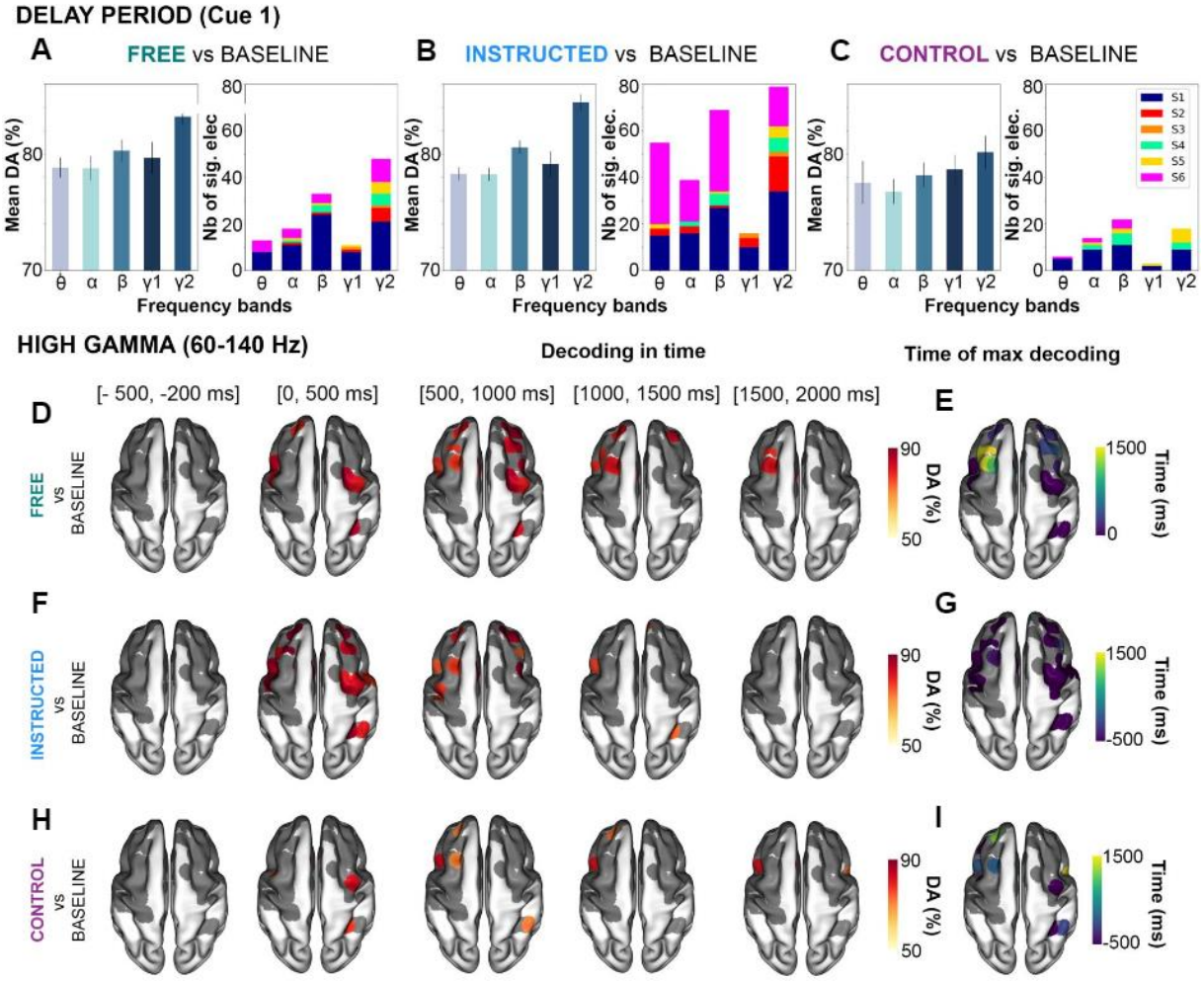

Figure 3. Single-trial classification of saccade planning and baseline activity using power modulations for the Free and Instructed conditions. A- C. Barplots of the mean decoding accuracies across subjects and significant electrodes for each frequency band (left panels, error bars represent the standard error of the mean) and summary of all significant electrodes by patient across frequencies showing that the largest clusters were found in high γ frequency range (right panels) for Free (A) and Instructed (B) and Control (C). **D**, **F**, **H**. Each column materializes regularly spaced time windows during the planning phase (-500 to 200 ms, 0 to 500 ms, 500 to 1000 ms, 1000 to 1500 ms and 1500 to 2000 ms). In **D, F** and **H**, electrodes with significant decoding accuracies ($p<0.01$, corrected with permutations using maximum statistics across electrodes, frequency bands and time) for all subjects are projected on the surface of the brain at different moments in time, while dark grey areas represent non-significant sites. In **E**, **G** and **I**, significant electrodes are colored depending on the timing at which significant electrodes could distinguish between baseline activity and post-stimulus activity during Free and Instructed conditions with the maximum decoding accuracy in the time-window [-500, 2000 ms].

Next, we directly compared the neural dynamics at play when planning an instructed saccade to that observed when planning a self-chosen saccade. This was again conducted by applying the LDA decoding framework during the delay period, but now directly classifying ***Free*** versus ***Instructed*** saccade trials, rather than comparing each to baseline pre-stimulus. Figures 4A-C show that the most prominent single-feature decoding (i.e. highest mean and maximum decoding accuracies and number of significantly decoding sites) was obtained when using HG activity as the feature (***Free vs Instructed***: mean HG DA = 77.4 %, max DA = 93.6 %). This was followed by the Beta band (***Free vs Instructed***: mean Beta DA = 74.1 %, max Beta DA = 82.5 %) across 5/6 participants (Figure 4A-C).

Interestingly, we found that HG and Beta were the only frequency bands to significantly discriminate ***Free*** vs ***Instructed*** conditions when using a multi-feature classification approach where observations across all electrode sites were combined into the decoding feature space ($p<0.01$, corrected for multiple comparisons across subjects, electrodes, frequencies and time points). The multi-site decoding accuracies for HG and Beta reached 86.8% (900 ms after Cue 1) and 75.6% (500 ms after Cue 1) respectively (see Figure 4C). Of note, figure 4D shows a plot of the HG power envelope over time (averaged across all sites with significant decoding). It suggests that HG power is stronger in the ***Instructed*** than in the ***Free*** condition earlier in time. Importantly, we see that over time, HG power then becomes higher for the ***Free*** saccade planning than for ***Instructed*** saccade planning during later stages of the delay period. Because this multi-site classification of free vs instructed saccade trials reveals that the most prominent predictor features were the HG and Beta bands, in the next two sections we will focus on the spatial distribution of the significantly decoding sites for these two bands specifically.

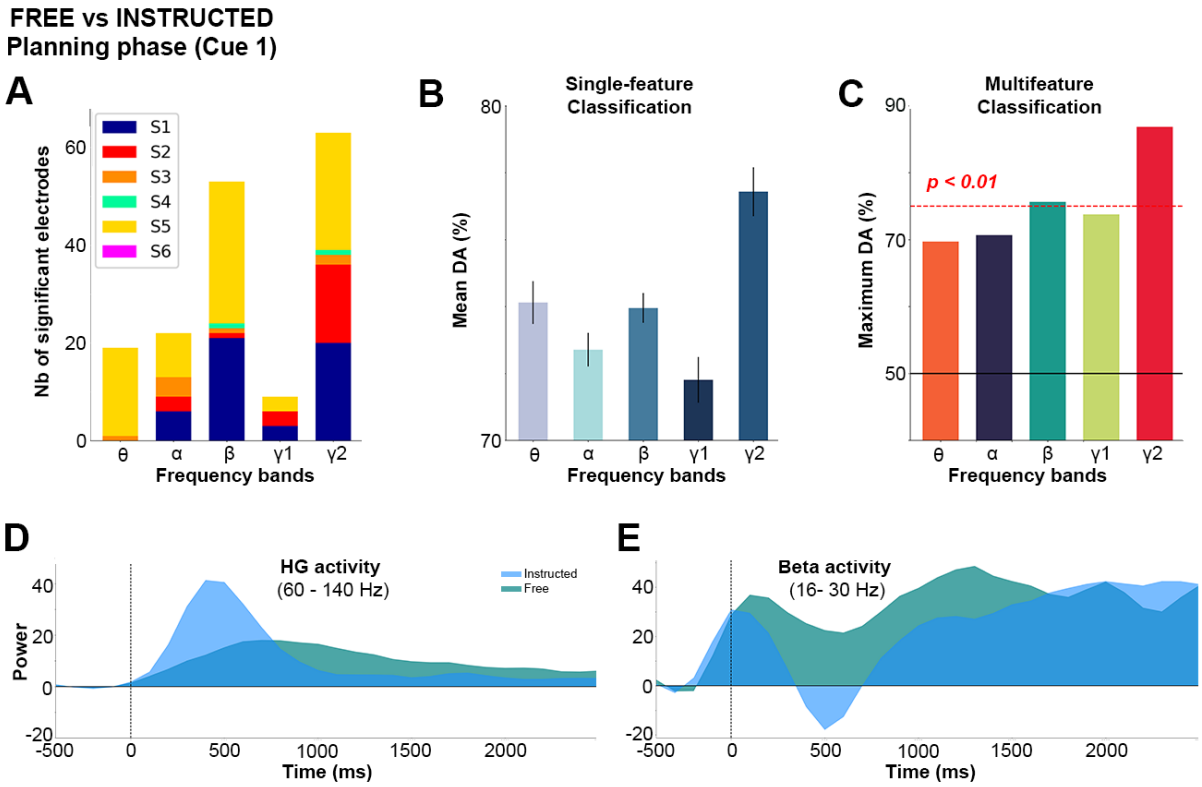

Figure 4. Single-trial classification Free and Instructed action selection during saccade planning using power modulations. A. Summary of all significant electrodes by patient across frequencies showing that the largest clusters were found in HG and β frequency bands. **B.** Barplots of the mean decoding accuracies across subjects and significant electrodes for each frequency band for Free vs Instructed single feature classification (error bars represent the standard error of the mean). **C.** Barplots of maximum decoding accuracies across subjects and significant electrodes for each frequency bands for Free vs Instructed multifeature classification. The black horizontal line represents the chance level, and the dashed horizontal red line represents the permutation threshold at $p < 0.01$ (corrected for multiple comparisons across subjects, electrodes, frequencies and time points). **D, E.** Time course of baseline corrected (-400 to -100 ms) HG activity (D) and beta power (E) aligned on Cue 1, for all electrodes significantly classifying Free and Instructed conditions.

Spatial distribution of enhanced high gamma power increases during free saccades

To identify the brain areas where HG increases indexed neural processing specific to free saccade decisions, we used a conjunction analysis (***Free*** > ***Control*** ∪ ***Free*** > ***Instructed***) applied to all electrode sites with significant classification of **free vs control** and **free vs instructed** trials during the first 2 seconds after Cue1. Figure 5 depicts the regions with significant decoding accuracies for all participants where the increase in HG activity was stronger during ***Free*** choice compared to both ***Control*** (Free > Control, see Figure 5A) and ***Instructed*** (Free > Instructed, see Figure 4C) trials. Figure 5B shows the conjunction of both results (for more details, see Figure S5). Specifically, we found that regions significantly involved in free choice (*p<0.01*, see STAR methods) were located in frontal areas such as FEF (2/6 subjects, 2 electrodes) and the superior frontal sulcus (2/6 subjects, 8 electrodes), as well as regions located in the superior part of the dorsal visual stream (1/6 subjects, 4 electrodes). Among all participants, the electrode with the

maximum decoding accuracy for both Free vs Control (88.6 %) and Free vs Instructed (81.4 %) conditions was situated in the right intraparietal sulcus (IPS) (S1, electrode derivation *p9-p8*, see Figure 5, last row of D-F). Power and decoding accuracy over time (Fig. 5D,F), time-frequency maps (Fig. 5E, upper rows) and single-trial plots (Figure 5E, lower rows), together highlight the sustained nature of HG activity during free saccade trials compared to the more transient increase of HG activity during planning instructed saccades. Moreover, we observe that the sustained HG activity during free choice decisions is more prominent in frontal areas than in parietal areas. Additionally, during the ***Control*** condition, parietal areas show an increase in HG activity (although weaker than during ***Free*** and ***Instructed*** conditions) while frontal areas do not. This might be due to the involvement of parietal regions in low-level sensory processing. Importantly, we found that our results are unlikely to be explained by lateralization effects since power time courses shown in Figure 5 did not differ when trials for left and right saccades were investigated separately (see Figure S4).

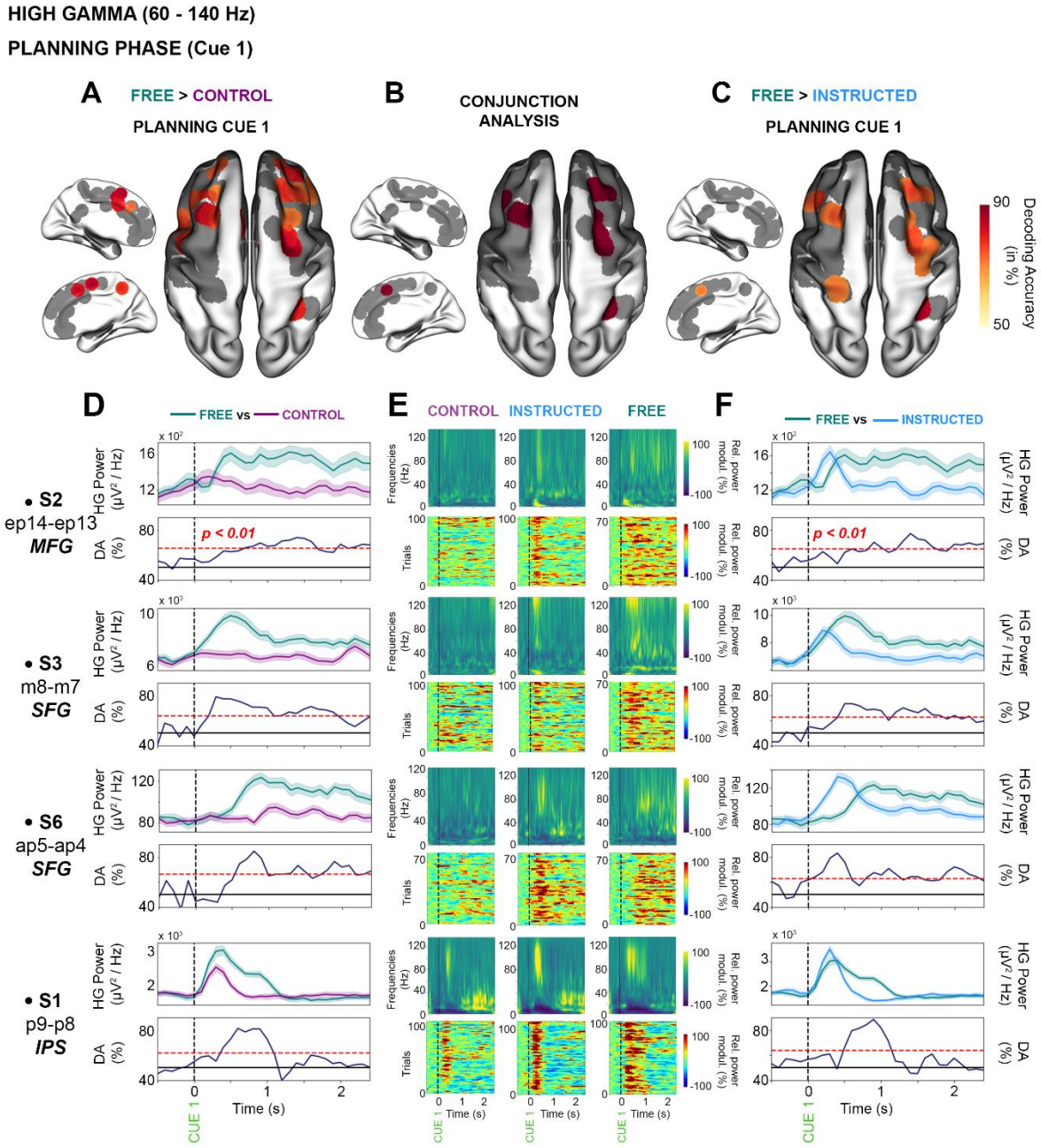

Figure 5. Single-trial HG activity decoding during Free saccade planning. In **A** and **C**, electrodes with significant decoding accuracies (*p<0.01, corrected with permutations using maximum statistics across electrodes, frequency bands and time*) for all subjects projected in color on the surface of the brain when HG activity is stronger in the ***Free*** condition than in the ***Control*** condition, respectively. We then isolated a network of regions specifically involved in ***Free*** decisions showed in **B** using a conjunction analysis (***Free*** > ***Control*** U ***Free*** > ***Instructed***). Dark grey areas represent non-significant electrodes. For four individual electrodes, we plotted power and decoding accuracy over time (**D** and **F**, red dotted lines indicate significance threshold at *p<0.01, corrected with permutations using maximum statistics across electrodes, frequency bands and time*), time-frequency-maps (**E**, upper row) and single-trial plots (**E**, lower row). In decoding accuracy plots, the continuous horizontal lines on the bar charts depict the theoretical chance level (50%), while the red dotted lines represent the statistical significance threshold ($p < 0.01$, corrected across time). This study allowed to isolate a network of regions specifically involved in free decisions showed in (**B**) using a conjunction analysis (*Free > Control* U *Free > Instructed*). We show that single electrodes are able to successfully decode ***Free*** vs ***Control*** and ***Free*** vs ***Instructed*** conditions (**D**) based on HG activity on a single-trial basis in frontal and parietal brain regions. Furthermore, time-frequency maps and single-trial plots inform us on the sustained nature of the HG activity increase during ***Free*** decisions compared to a more transient HG increase in the ***Instructed*** condition.

Spatial distribution of transient Beta power suppression during instructed saccades

To probe the involvement of Beta power suppression during the delay period across the three trial types, we conducted the same analyses as presented in the previous section for HG activity. Combining the conjunction analysis (***Instructed*** < ***Control*** ∪ ***Instructed*** < ***Free***) with the classification results we found that regions that were specific to instructed saccade preparation ($p < 0.01$, see STAR methods) were mostly located in areas belonging to the somatomotor network (2/6 subjects, 17 electrodes) and in FEF (2/6 subjects, 8 electrodes), and that the electrode with the maximum decoding accuracy for both Instructed vs Control (84 %) and Instructed vs Free (81 %) conditions was situated in the right FEF (Electrode b9-b8, see Figure 6, first row of D, E and F). The power and decoding accuracy over time (Fig 6D, F), time-frequency maps (Fig 6E, upper row) and single-trial plots (Fig 6E, lower row), illustrate the robustness of the beta suppression specifically during preparation of instructed saccades, compared to free choice and control conditions. Again, our results could not be explained by a lateralization effect (see Fig S4).

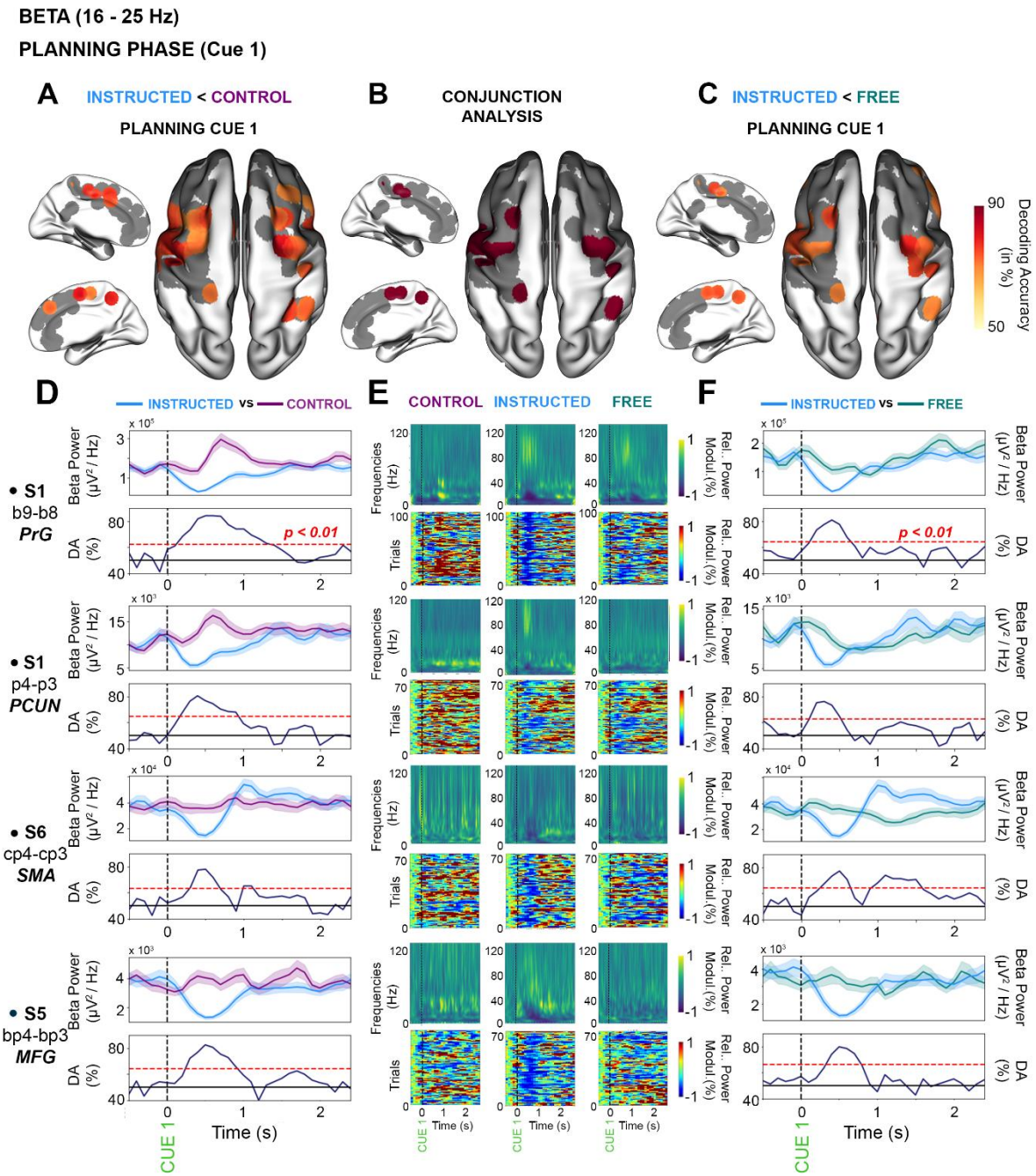

Figure 6. Single-trial β power decoding during Instructed saccade planning. In **A** and **C**, electrodes with significant decoding accuracies (*p<0.01, corrected with permutations using maximum statistics across electrodes, frequency bands and time*) for all subjects projected in color on the surface of the brain when β power is lower in the ***Instructed*** condition than in the ***Control*** condition and in the ***Free*** condition, respectively. We isolated a network of regions specifically involved in ***Instructed*** saccadic planning showed in **B** using a conjunction analysis (***Instructed*** < ***Control*** U ***Instructed*** < ***Free***). Dark grey areas represent non-significant electrodes. For four individual electrodes, we plotted power and decoding accuracy over time (**D** and **F**), time-frequency-maps (**E**, upper row) and single-trial plots (**E**, lower row). In decoding accuracy plots, the continuous horizontal lines on the bar charts depict the theoretical chance level (50%), while the red dotted lines represent the statistical significance threshold ($p < 0.01$, corrected across time). We show that single electrodes are able to successfully decode ***Instructed*** vs ***Control*** and ***Instructed*** vs ***Free*** conditions (**D**) based on β power on a single-trial basis in motor brain areas. Furthermore, time-frequency maps and single-trial plots (**E**) inform us on the early β suppression that is specific to the ***Instructed*** condition.

Disentangling the correlates of oculomotor execution and oculomotor planning

Previous reports have shown that saccade execution in response to a go signal is associated with distributed increases in high gamma power (Lachaux et al., 2006a). Yet, it has been so far hard to determine whether such gamma activity reflects target selection, visuomotor transformations, motor planning, actual oculomotor commands or a combination thereof. Analyzing the execution component (cue 2) of our delayed saccade paradigm provides a convenient way to address this question. To this end, we conducted a supervised classification analysis on ***Free***, ***Instructed*** and ***Control*** conditions as above, but this time using data collected during saccade execution (0 to 1500 ms after Cue 2). We found very few significant differences between saccade execution in the ***Free*** and ***Instructed*** conditions (Figure 7A), but neuronal oscillations could significantly differentiate the ***Control*** condition from the ***Instructed*** condition (Figure 7B) and from the ***Free*** condition (Figure 7C) in fronto-parietal cortical areas. Moreover, the largest clusters of significant electrodes, as well as the highest maximum decoding accuracies appeared in the HG frequency band (***Control vs Instructed***: max DA = 83.3 %; ***Control vs Free:*** max DA = 85.7 %, see Figure 7D, E). In a nutshell, our results show that HG power modulations during saccade execution were very similar whether the saccade was instructed or self-chosen. However, HG activity associated with saccade execution in the control condition (no previous planning possible) was significantly different than both ***Free*** and ***Instructed*** saccades (Figure 1B, D). These results seem to be consistent with the fact that no significant reaction time differences were found between ***Free*** and ***Instructed*** conditions (p = 0.48), while mean reaction time across participants significantly differed between the ***Control*** condition compared to both ***Free*** ($p = 5.51^{-8}$) and ***Instructed*** ($p = 5.39^{-7}$) conditions (Figure 1D). This led us to specifically investigate the nature of the relationship between reaction times and HG activity changes during saccade execution in regions that significantly differed between ***Control*** versus both ***Free*** and ***Instructed*** conditions. We first used a conjunction analysis to identify these regions (significant in 2/5 subjects at $p < 0.01$, and in 5/5 subjects at $p < 0.05$, see Figure 7C). Then, we computed Spearman's rank correlation coefficients between reaction times (i.e., latency of saccade onset) and the latency of HG peak for each trial in the three experimental conditions. By plotting the mean time courses (Fig 7E, H, K) and single trial plots of HG activity (Fig 7G, J M), we observed that the temporal dynamics and correlations between RTs and the latency of HG peaks were substantially different depending on the location of the electrodes. More specifically, we observe that significant electrodes located in the superior part of the dorsal visual stream (4 significant electrodes, 1/5 subject), HG peaks and reaction times were not significantly correlated (Figure 7F, G) (Electrode m13-m12; ***Control*** [p = 0.311, Rcoef =0.1], ***Free*** [p = 0.367, Rcoef = - 0.09] and ***Instructed*** [p = 0.968, Rcoef =- 0.01]),

although HG activity was significantly stronger in the ***Control*** condition compared to both ***Free*** and ***Instructed*** conditions (Figure 7E). For significant electrodes located in the frontal eye field and in the pre supplementary area (5 significant electrodes, 2/5 subject), we show that reaction times and HG peak latencies were significantly correlated in all three conditions (Figure 7I; Electrode j5-j4; ***Control*** [p = 0.001, Rcoef =0.32], ***Free*** [p = 0.003, Rcoef =0.29] and ***Instructed*** [p = 0.041, Rcoef =0.2]). These findings are consistent with the well-established conclusion that the frontal eye field is involved in saccade execution. This also demonstrates that the significant changes in HG peak latencies we found (Figure 7J) are tightly related to reaction times. In other words, faster reaction times during saccade execution when a decision was already made during the planning phase correspond to earlier peaks in HG activity in the frontal eye field (Figure 7H). In more anterior regions of the brain such as the superior and middle frontal gyri (5 significant electrodes, 1/5 subject), we observed HG increases during saccade execution only when a decision wasn't made during the planning phase (***Control*** condition, see Figure 7E), which was correlated with reaction times (Electrode f8-f7; ***Control*** [p = 0.009, Rcoef =0.26], ***Free*** [p = 0.011, Rcoef =0.25] and ***Instructed*** [p = 0.477, Rcoef =0.07]; Electrode m13-m12; ***Control*** [p = 0.002, Rcoef =0.3], ***Free*** [p = 0.918, Rcoef = -0.01] and ***Instructed*** [p = 0.284, Rcoef =0.1]]).

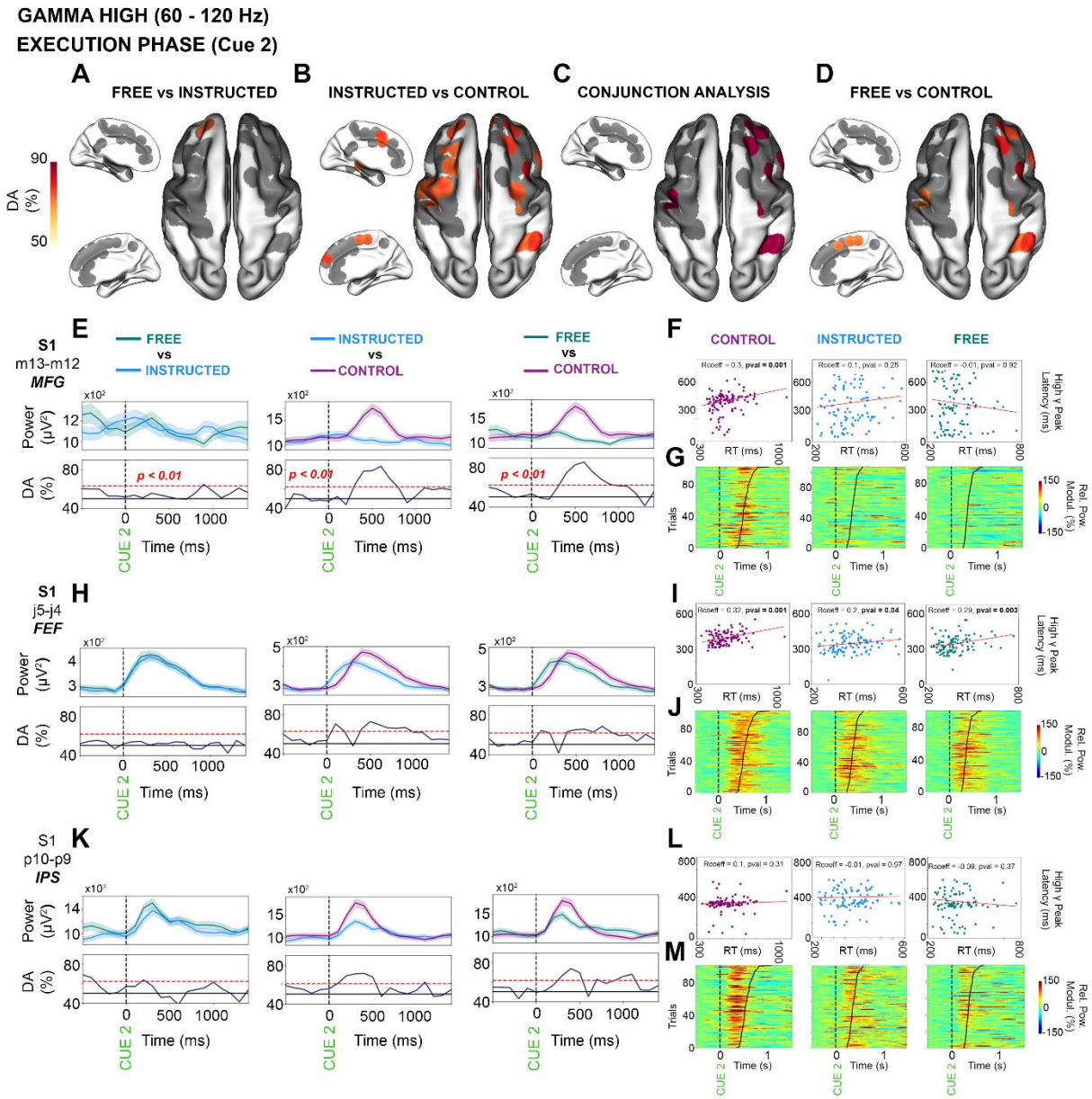

Figure 7. Single-trial HG activity decoding during saccade execution. We compared high frequency neuronal activity (HG: 60-140hz) of saccade execution (0 to 1500 ms after Cue 2) between ***Free*** and ***Instructed*** (**A**), ***Instructed*** and ***Control*** (**B**), and ***Free*** vs ***Control*** (**D**) (*p<0.01, corrected with permutations using maximum statistics across electrodes, frequency bands and time*) for all subjects projected in color on the surface of the brain. **C**. We isolated a network of regions specifically involved in saccadic execution when no action selection occurred during the planning phase (***Control*** condition) using a conjunction analysis (***Control*** *vs* ***Instructed*** U ***Control*** *vs* ***Free***). For three individual electrodes, we plotted power and decoding accuracy over time (**E, H, K**). In decoding accuracy plots, the continuous horizontal lines on the bar charts depict the theoretical chance level (50%), while the red dotted lines represent the statistical significance threshold ($p < 0.01$, corrected across time). **F, I, L.** Scatter plots showing correlations between reaction times and HG peak latency. **G**, **J**, **M.** Single-trial plots showing relative power modulations of HG activity for three different electrodes and for each of the three conditions during saccade execution. Thick dark lines represent the sorted reaction times for each trial.

Discussion

For the first time, we provide direct recordings of neural dynamics underlying oculomotor decision-making in the human brain using intracranial EEG. Our results confirm the hypothesis that oculomotor decision processing (i.e. a free choice saccade) in humans is associated with changes in LFPs –especially high frequency activity- across a parieto-frontal network. In particular, our single-trial classification framework revealed that the achieved discrimination accuracy between instructed and free saccade conditions was highest when using high frequency activity as feature, compared to using spectral power in lower frequency bands. Interestingly, the temporal dynamics of the LFPs revealed that free choice trials were associated with a more sustained induced HG response than instructed saccade trials which in turn showed a more transient HG response and an enhanced beta suppression.

In each of the six human participants, freely deciding where to look was associated with enhanced sustained broadband HG activity in a decision network including frontal and parietal brain areas. These effects were robustly observed at the level of single trials with iEEG. The large frequency bandwidth of the HG band responses reported here have been suggested to reflect a global enhancement of the local neuronal firing in the underlying cortical tissue, observed as a "spike bleedthrough" in the field power spectra (Kucewicz et al., 2017; Manning et al., 2009; Mukamel et al., 2005; Nir et al., 2007; Ray and Maunsell, 2011; Ray et al., 2008). Our findings support the view that HG activity is likely to stem from the nature of the cumulative discharge rate of local neuronal networks in the superficial cortical layers integrated over time and neural populations recorded with iEEG (Leszczynski and Schroeder, 2019; Manning et al., 2009; Mukamel et al., 2005; Ray and Maunsell, 2011; Ray et al., 2008). In animals, single-unit studies found sustained neuronal activity in parietal (Chafee and Goldman-Rakic, 1998; Goard et al., 2016; Huang et al., 2013; Kim and Shadlen, 1999; Rainer et al., 1999; Riley and Constantinidis, 2015; Romo and de Lafuente, 2013; Siegel et al., 2015; Stokes, 2015) areas during decision-making, working memory and response selection tasks featuring pre-defined delay periods. Interestingly, this persistent neuronal firing was also found in a free choice oculomotor task (Platt and Glimcher, 1999). Given that increases in neuronal firing have been shown to be correlated with increases in HG activity (Manning et al., 2009; Mukamel et al., 2005; Niessing et al., 2005; Whittingstall and Logothetis, 2009), the principal finding of the present study, i.e. the sustained HG activity, appears to mirror -in humans- the persistent single-unit neural firing previously demonstrated in non-human primates.

Recent research indicates a putative role for sustained prefrontal cortex HG activity in linking stimulus perception with action execution (Haller et al., 2018). Interestingly, this persistent (stimulus to response) HG activity was observed across a diverse range of cognitive tasks and interpreted as a common functional substrate for information integration and response selection. Using a fully data-driven approach, our results extend these observations to the specific case of free choice. Furthermore, several other invasive and non-invasive human electrophysiological studies have shown the importance of HG activity in the active maintenance of relevant information in short-term memory (Jensen et al., 2007; Jokisch and Jensen, 2007; Roux et al., 2012; Tallon-Baudry et al., 1998) and in perceptual decision-making (Donner et al., 2009). In the light of the aforementioned findings and existing theories of action selection (Cisek and Kalaska, 2005; Costello et al., 2013; Coulthard et al., 2008; Cui and Andersen, 2007; Oliveira et al., 2010;

Pastor-Bernier and Cisek, 2011; Pastor-Bernier et al., 2012; Shadlen and Newsome, 2001), we propose that sustained HG activity in frontal and parietal areas during free saccade planning in the present task may reflect persistent neuronal firing that helps maintain enhanced competition between various potential movement plans with equal rewarding outcomes compared to a single movement plan in instructed saccades (cf. Cisek and Kalaska, 2010). This may, in turn, subserve the capacity of flexibly choosing and switching between alternatives during free choice (i.e., being able to change one's mind). Moreover, the involvement of the fronto-parietal network is consistent with the brain structures implementing action selection (free choice) when maximally competing alternatives are present, both in humans (Carl et al., 2016; Haggard, 2008; de Jong, 2011; Kable and Glimcher, 2009) and in monkeys (Gold and Shadlen, 2007; Pesaran et al., 2008).

Moreover, the involvement of frontal and parietal cortex in free action selection has been previously documented in human fMRI studies (Beudel and de Jong, 2009; Khonsari et al., 2007; Milea et al., 2007; Oliveira et al., 2010; Soon et al., 2008). Importantly, the decision process of where to look when facing two possible visual targets was found to be specifically associated with frontal-lobe activation in the dorsolateral prefrontal cortex, as well as in frontal eye fields in an fMRI study using the same experimental paradigm (Milea et al., 2007). The correspondence between BOLD responses and iEEG HG activity in the same task further supports previous findings that broadband HG activity band modulations co-localize with BOLD variations in humans (Kayser et al., 2004; Lachaux et al., 2007, 2012; Logothetis et al., 2001; Mukamel et al., 2005; Niessing et al., 2005; Ojemann et al., 2013).

During instructed saccades, we observed a fast and transient increase in HG activity in fronto-parietal brain areas, accompanied by an early β suppression in motor areas. Based on previous human studies using delayed saccade tasks (Medendorp et al., 2006; Van Der Werf et al., 2008; Van der Werf et al., 2009), this may reflect the rapid encoding of a motor plan after presenting the instructional cue. The role of β oscillations is thought to maintain the status-quo of current cognitive or sensorimotor states (Engel and Fries, 2010; Gilbertson et al., 2005; Pfurtscheller et al., 1996), and its desynchronization has been associated with activation of sensorimotor areas during motor planning and execution (Crone et al., 1998; Murthy and Fetz, 1992; Pfurtscheller and Lopes da Silva, 1999; Sanes and Donoghue, 1993). Given our results, we interpret the early suppression of β in motor areas during the planning of instructed saccade as a way to ''break the status quo'', and reflects the change of the motor system from a resting state to a state closer to the one associated with action execution, leading to a faster encoding of a motor plan. Conversely, the fact that β power is not suppressed during free and control conditions might reflect the absence of clear-cut motor preparation signals.

It is noteworthy to consider that our findings in the HG band are consistent with MEG results obtained in the only study in which the authors investigated the role of neuronal oscillations in a delayed saccade task (Carl et al., 2016). In our study, we extend these findings by using the combined spatial and temporal resolution of iEEG (allowing us to investigate higher frequencies up to 140 hz), and by using a data-driven approach to characterize neural dynamics during free choice decisions at the single-trial level. This is an important step towards a better understanding of the neural correlates subserving internally motivated decisions in humans. However, Carl et al. found a stronger decrease in α and β bands during free saccade target selection compared to instructed saccades, while our results indicate a stronger β suppression during planning of instructed saccades. These conflicting results could be explained by differences between the two

tasks, since participants in the study of Carl et al. were asked to perform a guided saccade to one of 16 targets indicated by a color change to either green (***Free*** condition) or green with a red marker (***Instructed*** condition). Thus, differences in β oscillations during planning could be due to the number of alternatives, or to physical differences between cue colors affecting sensory responses. Additionally, the authors did not include a ***Control*** condition in the design of their experimental paradigm and couldn't precisely quantify changes due to sensory processes.

Finally, we found that during saccade execution (after the Go signal), saccade onset latencies and HG activity in a distributed network of frontal and parietal brain differed depending on whether there was any kind of action selection during the planning phase. This led us to investigate the nature of the relationship between saccade onset latencies and the latency of HG peak activity during saccade execution. We found different patterns of HG activity depending on electrode locations, which were in line with recent theories of action selection such as the affordance competition hypothesis (Cisek, 2007; Cisek and Kalaska, 2010). This theory makes specific predictions on the role of frontoparietal areas in the specification of potential actions during movement execution, and can be used to shed light on the neural mechanisms underlying the configuration of oculomotor commands in humans. First, during saccade execution, we showed that HG activity in regions located in the superior part of the dorsal visual stream is significantly stronger when subjects are not asked to make a decision (i.e., instructed saccade condition). Moreover, we found that increases in the latency of the peak HG activity were not correlated with the timing of the saccade execution. According to Goodale & Milner (1992), the dorsal visual stream can be considered as part of the system for specifying the parameters of potential actions using visual information, a process that continues during movement execution (Resulaj et al., 2009). Specifically, the intraparietal sulcus has been identified in the preparation and the redirection of movements and movement intentions (i.e., motor attention, see Rushworth et al., 2003). Thus, the absence of correlation between HG peak latency and saccade onset in our task suggests that the superior part of the dorsal visual stream is involved in action specification by allocating visuospatial attention resources (i.e., acting as an attentional filter sensitive to spatial information), but is not directly involved in saccadic motor control. The fact that HG activity was weaker when decisions were made during the planning phase might indicate that part of the attentional filtering has been done already and does not need to be entirely reactivated during saccade execution. The superior part of the dorsal visual stream is highly interconnected with other parts of the gaze control system including the frontal eye fields. In this study, since the latency of HG peak activity was correlated with reaction times in frontal eye fields, our results seem to confirm its involvement in performing the visuomotor transformation to generate a saccade plan internally in humans (Lachaux et al., 2006b; Sendhilnathan et al., 2017). Moreover, we show that when oculomotor planning processes were engaged during the delay period, HG activity in frontal eye fields increased earlier than when participants did not prepare any saccade (control), thus allowing to generate saccades faster. Lastly, we observed very different patterns of neuronal activity in more anterior regions of the brain such as the middle and superior frontal gyri, in which HG activity during saccade execution only increased when no action selection processes were engaged during the planning phase since in the ***Control*** condition, no directional information was available until the GO signal. This indicates that once oculomotor plans are made, the involvement of the middle and superior gyri are no longer needed for the execution of saccades. However, if a saccade wasn't planned, the latency of the peak of HG activity was correlated with reaction times. This suggests that middle and superior frontal gyri are also involved in the execution of saccades (Cameron et al., 2015).

Of note, participants in our study were neurosurgical patients with drug resistant epilepsy. We controlled this potential bias by following previously used routine procedures (Bastin et al., 2017; Jerbi et al., 2009; Ossandón et al., 2011) such as careful visual inspection and removal of signals showing typical epileptic waveforms (e.g., epileptic spikes), this might limit the generalizability to healthy subjects. Moreover, compared to previous non-invasive studies based on non-invasive recordings such as magnetoencephalography (MEG), the direct intracranial recordings used here allow for a higher spatial resolution particularly for deeper structures, a higher signal-to-noise ratio that is crucial to perform single-trial analyses, and the detection of electrophysiological correlates of decision making at higher frequencies (up to 140 Hz). But this comes at the cost of heterogenous spatial sampling among patients, inherent to all iEEG studies. The electrode implantation across the six participants (see Figure 1B, C) yielded a reasonable coverage of frontal and central areas, but the posterior parietal cortex was under-represented and none of our patients were implanted in the occipital cortex. Lastly, studies have shown that artifacts caused by microsaccades may contaminate iEEG recordings (Jerbi et al., 2009). However, based on the localization, the frequency range and the time-course of HG activity, the current recordings of HG activity do not appear to be attributable to ocular artifacts.

To conclude, the present study provides the first direct electrophysiological investigation of eye movement decisions using depth recordings in humans. Our finding that free oculomotor decisions are associated with sustained HG activity in a parieto-frontal network bridges the gap between findings in human and non-human primates and expands our understanding of the spatial, temporal and spectral dynamics of human decision making.

Acknowledgments

We thank P. Cisek and A. Green for valuable discussions and comments. K.J. is supported by funding from the Canada Research Chairs program and a Discovery Grant (RGPIN-2015-04854) from the Natural Sciences and Engineering Research Council of Canada, a New Investigators Award from the Fonds de Recherche du Québec - Nature et Technologies (2018-NC-206005) and an IVADO- Apogée fundamental research project grant. T.T. was supported by IVADO Excellence Scholarship – PhD. This work was supported in part by the EU research programs NeuroBotics (FET FP6-IST001917) and NeuroProbes (FP6-IST 027017).

Methods

Contact for Reagent and Resource Sharing

All requests for further information and resources should be directed to and will be fulfilled by the Lead Contact, Thomas Thiery (thomas.thiery@umontreal.ca).

Experimental Model and Subject Details

Six patients with drug-resistant epilepsy participated in this study (6 females, mean age 30.3 ± 9.6). The patients were stereotactically implanted with multisite EEG depth electrodes at the Epilepsy Department of the Grenoble Neurological Hospital (Grenoble, France). In collaboration with the medical staff, and based on visual inspection, electrodes presenting pathological waveforms were discarded from the present study. All patients had normal vision without corrective glasses. All participants provided written informed consent, and the experimental procedures were approved by the local Ethical Committee (''ISD et SEEG'' project, CPP Sud-Est V n° 09-CHU-12).

Method Details

Electrode implantation and stereotactic EEG recordings

Each patient was implanted with stereotactic electroencephalography (SEEG) electrodes (diameter of 0.8 mm). Depending on the implanted structure, electrodes were composed of 10 to 15 contacts that were 2 mm wide and 1.5 mm apart (DIXI Medical Instrument, Besançon, France). Intracranial EEG signals were recorded from a total of 778 intracerebral sites across all patients (Between 128 and 133 sites per participant). At the time of acquisition, a white matter electrode was used as reference, and data was sampled at 1024 Hz and bandpass filtered between 0.1 and 250 Hz. Electrode locations were determined in each individual participant using the stereotactic implantation scheme and the Talairach and Tournoux proportional atlas (Talairach and Tournoux, 1988). The coordinates of each electrode contact are given following these references: origin (anterior commissure), anteroposterior axis (anterior commissure - posterior commissure), and vertical axis (interhemispheric plane). The electrodes were then localized in each individual subject using Talairach coordinates, and then transformed to standard MNI coordinate system (Figure 1C).

Delayed motor task

For each trial, participants were instructed to perform horizontal saccades toward one of the two targets, depending on a visually presented central cue appearing briefly for 250 ms (*Planning phase*). In the *FREE* condition, the cue (outline diamond-shaped) indicated the participants freedom to decide the direction (Right or Left) of the forthcoming intentional saccade. In the *INSTRUCTED* condition, participants prepared an saccade towards the target indicated by the cue (empty arrow). After a variable delay (3750, 5750 or 7750 ms) during which the participants prepared the (chosen or instructed) saccade while fixating a central fixation point, a GO signal (a central filled double-arrow in the *FREE* condition and an arrow pointing to one of the two targets in the *INSTRUCTED* condition) indicated that the participants could execute the saccade (*Execution phase*). In the *CONTROL* condition, an empty central rectangle indicated that the participants could continue central fixation without preparing any forthcoming saccade. This *CONTROL* condition was then followed after a variable delay (3750, 5750 or 7750 ms) by a *GO* signal indicating the direction of the saccade to be executed immediately, i.e. without prior

preparation. After every saccade execution, participants had to fixate the central fixation point immediately.

Behavioral analysis

Based on the EOG traces (see Figure S2), we computed reaction times for each trial and for all participants in the ***Control***, ***Instructed*** and ***Free*** conditions. In order to test whether reaction times differed significantly across conditions, we used a paired permutation pseudo Student's t-test and compared reaction times for ***Control*** vs ***Instructed***, ***Control*** vs ***Free***, and ***Instructed*** vs ***Free*** conditions.

EOG Data preprocessing

Oculomotor performance was followed online using horizontal and vertical electro-oculograms (EOG), allowing to measure the amplitude and the speed of saccades (see Figure S2), as well as the errors made by each subject. Four electrodes placed around the eyes to measure horizontal and vertical eye movements with a sampling frequency of 1024 Hz.

SEEG Data preprocessing

SEEG data preprocessing was conducted according to our routine procedures (Bastin et al., 2017; Jerbi et al., 2009). These included signal bipolarization, where each electrode site was re-referenced to its direct neighbor. Bipolar re-referencing can increase sensitivity and reduce artefacts by canceling out distant signals that are picked up by adjacent electrode contacts (e.g. mains power). The spatial resolution of bipolar SEEG electrodes was approximately 3 mm (Jerbi et al., 2009; Lachaux et al., 2003). Next, using visual inspection and time-frequency explorations of the signal, we excluded electrodes containing pathological epileptic activity. The pre-processing led to a total of 543 bipolar derivations across all participants (see Figure 1B).

Quantification and Statistical Analysis

Spectral analyses

We conducted power analyses in several standard frequency bands defined as follows: theta (θ) [4–8 Hz], alpha (α) [8–15 Hz], beta (β) [16–30 Hz], low gamma (low γ) [30–60] and HG [60-140 Hz]. This was achieved by first filtering the raw EEG signals using a finite impulse response filtering (FIR1, order = 3) and then computing the Hilbert transform over 250 ms time windows with an overlap of 100 ms. The power features used for classification were computed as mean power over 250 ms time windows with an overlap of 100 ms during planning (-500 ms to 2500 ms), where t=0 ms corresponds to the onset of Cue 1, and execution (-500 ms to 1500 ms) where t=0 ms corresponds to the onset of Cue 2. The classification was applied on unnormalized power. Whenever present, baseline normalization was only used for visualization purposes (time-frequency maps and single trial representation). Baseline normalization was achieved for each frequency band, by subtracting then dividing by the mean of a 400 ms baseline window, i.e. the pre-stimulus rest period ([-500ms, -100 ms]).

Signal classification

We set out to explore the feasibility of using multi-site human Local Field Potential (LFP) data (543 bipolar electrode sites) to perform classifications during motor planning and execution. To this end, we implemented a machine learning (ML) framework for trial-by-trial classification using spectral power. Several classification techniques were initially tested for the single feature classification procedure, including linear-discriminant analysis (LDA), k-nearest-neighbor (KNN) and support vector machine (SVM). The classification accuracy results were very similar across the 3 methods. The LDA algorithm (Fisher, 1936) was the fastest and was therefore chosen for this study given the computationally-demanding permutation tests used to evaluate classifier performance. In brief, for a two-dimensional problem, the LDA algorithm tries to find a hyperplane that maximizes the mean distance between the mean of the two classes while minimizing inter-class variance.

Decoding accuracy and statistical evaluation of decoding performance

Single-trial classification performance was evaluated in each participant separately. We used a standard stratified 10-fold cross-validation approach with Scikit-learn, a Python 3 package dedicated to machine-learning analyses (Pedregosa et al., 2012). First, the data set was pseudo-randomly split into 10, equally-sized, observations: 9 segments were used for training the classifier, and the last one as the test set. This procedure was repeated 10 times, such that every observation in the data was used exactly once for testing, and at least once for training, but never at the same time. This strict separation of training and testing ensures the test data was naïve and did not violate basic classification principles (e.g. Lemm et al., 2011). The use of stratification seeks to ensure that the relative proportion of labels (or classes) in the whole data set is reasonably preserved within each of the segments after the split. Next, the performance of the achieved decoding was calculated using the decoding accuracy (DA) metric, which was computed as the mean correct classification across all folds. The statistical significance of the obtained decoding accuracies was evaluated by computing statistical thresholds using permutation tests ($n=100$, $p<0.01$). In other words, a null-distribution is generated by repeatedly ($n=100$) computing the classification accuracy obtained after randomly permuting class labels (Combrisson and Jerbi, 2015). In all our decoding analyses, we used maximum statistics to correct across electrodes, frequency bands and time with a statistical threshold at $p<0.01$.

Multifeature classification analysis

To perform the multi-feature analysis, we use the Exhaustive Feature Selection (EFS) method from mlxtend (Raschka, 2018) applied for each frequency band, for each subject. The EFS algorithm will test all the possible combination of the frequency bands and will select which feature or set of features allows for better decoding of our two conditions (***Free*** vs ***Instructed***). The feature selection is scored on a stratified validation dataset consisting of one third of the data. The EFS is repeated with all possibilities of validation set and the best selected features are counted for each electrode.

Correlations between reaction times and HG activity

We computed Spearman's rank correlation coefficients between reaction times and the latency of HG peak of activity for each trial in the three Free, Instructed and Control conditions during saccade execution. The statistical significance was established by using a two-sided test whose null hypothesis is that two sets of data are uncorrelated. The p-value thus indicates the probability of an uncorrelated system producing datasets that have a Spearman correlation at least as extreme as the one computed from these datasets.

Data mapping to a 3-D standard cortical representation

To facilitate the interpretation of the results, all significant task-based feature modulations and decoding results were remapped from the intracranial electrode sites onto a standard cortical representation. To achieve this, all electrode coordinates were transformed from individual Talairach space to standard MNI space using Visbrain (Combrisson et al., 2019), an open-source Python 3 package dedicated to brain signals visualization, to project the data from SEEG sites onto the cortical surface. In practice, data from the iEEG electrodes were assigned to the vertices on the MNI cortical mesh that fell within a fixed radial distance of 10 mm from each electrode. This cortical representation technique is methodologically consistent with methods used in previous iEEG studies (Bastin et al., 2017; Jerbi et al., 2009; Ossandón et al., 2012). In addition to generating brain-wide visualization of all significant features and decoding performances, this method was also used to display the cortical coverage provided by all the electrodes in this study (dark gray areas in Figure 3, Figure 4, Figure 5 and Figure 6).

Data and Software Availability

Electrophysiological data were analyzed using Python 3, in conjunction with toolboxes including Visbrain (Combrisson et al., 2019) for data visualisation and Scikit-learn (Pedregosa et al., 2012) for machine learning analyses. Data and custom Python analysis scripts are available upon reasonable request from Thomas Thiery (thomas.thiery@umontreal.ca).

References

Anderson, E.J., Jones, D.K., O'Gorman, R.L., Leemans, A., Catani, M., and Husain, M. (2012). Cortical network for gaze control in humans revealed using multimodal MRI. Cereb. Cortex N. Y. N 1991 *22*, 765–775.

Basso, M.A., and Wurtz, R.H. (1998). Modulation of neuronal activity in superior colliculus by changes in target probability. J. Neurosci. Off. J. Soc. Neurosci. *18*, 7519–7534.

Bastin, J., Lebranchu, P., Jerbi, K., Kahane, P., Orban, G., Lachaux, J.-P., and Berthoz, A. (2012). Direct recordings in human cortex reveal the dynamics of gamma-band [50-150 Hz] activity during pursuit eye movement control. NeuroImage *63*, 339–347.

Bastin, J., Deman, P., David, O., Gueguen, M., Benis, D., Minotti, L., Hoffman, D., Combrisson, E., Kujala, J., Perrone-Bertolotti, M., et al. (2017). Direct Recordings from Human Anterior Insula Reveal its Leading Role within the Error-Monitoring Network. Cereb. Cortex N. Y. N 1991 *27*, 1545–1557.

Beudel, M., and de Jong, B.M. (2009). Overlap and segregation in predorsal premotor cortex activations related to free selection of self-referenced and target-based finger movements. Cereb. Cortex N. Y. N 1991 *19*, 2361–2371.

Blanke, O., and Seeck, M. (2003). Direction of saccadic and smooth eye movements induced by electrical stimulation of the human frontal eye field: effect of orbital position. Exp. Brain Res. *150*, 174–183.

Brody, C.D., Hernández, A., Zainos, A., and Romo, R. (2003). Timing and Neural Encoding of Somatosensory Parametric Working Memory in Macaque Prefrontal Cortex. Cereb. Cortex *13*, 1196–1207.

Cameron, I.G.M., Riddle, J.M., and D'Esposito, M. (2015). Dissociable Roles of Dorsolateral Prefrontal Cortex and Frontal Eye Fields During Saccadic Eye Movements. Front. Hum. Neurosci. *9*.

Carl, C., Hipp, J.F., König, P., and Engel, A.K. (2016). Spectral Signatures of Saccade Target Selection. Brain Topogr. *29*, 130–148.

Chafee, M.V., and Goldman-Rakic, P.S. (1998). Matching patterns of activity in primate prefrontal area 8a and parietal area 7ip neurons during a spatial working memory task. J. Neurophysiol. *79*, 2919–2940.

Cisek, P. (2007). Cortical mechanisms of action selection: the affordance competition hypothesis. Philos. Trans. R. Soc. B Biol. Sci. *362*, 1585–1599.

Cisek, P., and Kalaska, J.F. (2005). Neural correlates of reaching decisions in dorsal premotor cortex: specification of multiple direction choices and final selection of action. Neuron *45*, 801–814.

Cisek, P., and Kalaska, J.F. (2010). Neural mechanisms for interacting with a world full of action choices. Annu. Rev. Neurosci. *33*, 269–298.

Coe, B., Tomihara, K., Matsuzawa, M., and Hikosaka, O. (2002). Visual and Anticipatory Bias in Three Cortical Eye Fields of the Monkey during an Adaptive Decision-Making Task. J. Neurosci. *22*, 5081–5090.

Combrisson, E., and Jerbi, K. (2015). Exceeding chance level by chance: The caveat of theoretical chance levels in brain signal classification and statistical assessment of decoding accuracy. J. Neurosci. Methods *250*, 126–136.

Combrisson, E., Vallat, R., O'Reilly, C., Jas, M., Pascarella, A., Saive, A.-L., Thiery, T., Meunier, D., Altukhov, D., Lajnef, T., et al. (2019). Visbrain: A Multi-Purpose GPU-Accelerated Open-Source Suite for Multimodal Brain Data Visualization. Front. Neuroinformatics *13*, 14.

Connolly, J.D., Goodale, M.A., Menon, R.S., and Munoz, D.P. (2002). Human fMRI evidence for the neural correlates of preparatory set. Nat. Neurosci. *5*, 1345–1352.

Costello, M.G., Zhu, D., Salinas, E., and Stanford, T.R. (2013). Perceptual Modulation of Motor—But Not Visual—Responses in the Frontal Eye Field during an Urgent-Decision Task. J. Neurosci. *33*, 16394–16408.

Coulthard, E., Rudd, A., and Husain, M. (2008). Motor neglect associated with loss of action inhibition. J. Neurol. Neurosurg. Psychiatry *79*, 1401–1404.

Crone, N.E., Miglioretti, D.L., Gordon, B., and Lesser, R.P. (1998). Functional mapping of human sensorimotor cortex with electrocorticographic spectral analysis. II. Event-related synchronization in the gamma band. Brain J. Neurol. *121 (Pt 12)*, 2301–2315.

Cui, H., and Andersen, R.A. (2007). Posterior Parietal Cortex Encodes Autonomously Selected Motor Plans. Neuron *56*, 552–559.

Donner, T.H., Siegel, M., Fries, P., and Engel, A.K. (2009). Buildup of Choice-Predictive Activity in Human Motor Cortex during Perceptual Decision Making. Curr. Biol. *19*, 1581–1585.

Dorris, M.C., and Glimcher, P.W. (2004). Activity in posterior parietal cortex is correlated with the relative subjective desirability of action. Neuron *44*, 365–378.

Engel, A.K., and Fries, P. (2010). Beta-band oscillations--signalling the status quo? Curr. Opin. Neurobiol. *20*, 156–165.

Fisher, R.A. (1936). The Use of Multiple Measurements in Taxonomic Problems. Ann. Eugen. *7*, 179–188.

Forgacs, P.B., von Gizycki, H., Selesnick, I., Syed, N.A., Ebrahim, K., Avitable, M., Amassian, V., Lytton, W., and Bodis-Wollner, I. (2008). Perisaccadic parietal and occipital gamma power in light and in complete darkness. Perception *37*, 419–432.

Frost, D., and Pöppel, E. (1976). Different programming modes of human saccadic eye movements as a function of stimulus eccentricity: Indications of a functional subdivision of the visual field. Biol. Cybern. *23*, 39–48.

Gilbertson, T., Lalo, E., Doyle, L., Di Lazzaro, V., Cioni, B., and Brown, P. (2005). Existing motor state is favored at the expense of new movement during 13-35 Hz oscillatory synchrony in the human corticospinal system. J. Neurosci. Off. J. Soc. Neurosci. *25*, 7771–7779.

Goard, M.J., Pho, G.N., Woodson, J., and Sur, M. Distinct roles of visual, parietal, and frontal motor cortices in memory-guided sensorimotor decisions. eLife *5*.

Gold, J.I., and Shadlen, M.N. (2007). The neural basis of decision making. Annu. Rev. Neurosci. *30*, 535–574.

Goodale, M.A., and Milner, A.D. (1992). Separate visual pathways for perception and action. Trends Neurosci. *15*, 20–25.

Haggard, P. (2008). Human volition: towards a neuroscience of will. Nat. Rev. Neurosci. *9*, 934–946.

Haller, M., Case, J., Crone, N.E., Chang, E.F., King-Stephens, D., Laxer, K.D., Weber, P.B., Parvizi, J., Knight, R.T., and Shestyuk, A.Y. (2018). Persistent neuronal activity in human prefrontal cortex links perception and action. Nat. Hum. Behav. *2*, 80–91.

Huang, Y., Matysiak, A., Heil, P., König, R., and Brosch, M. Persistent neural activity in auditory cortex is related to auditory working memory in humans and nonhuman primates. eLife *5*.

Jensen, O., Kaiser, J., and Lachaux, J.-P. (2007). Human gamma-frequency oscillations associated with attention and memory. Trends Neurosci. *30*, 317–324.

Jerbi, K., Hamamé, C.M., Ossandón, T., and Dalal, S.S. (2008). Role of Posterior Parietal Gamma Activity in Planning Prosaccades and Antisaccades. J. Neurosci. *28*, 13713–13715.

Jerbi, K., Ossandón, T., Hamamé, C.M., Senova, S., Dalal, S.S., Jung, J., Minotti, L., Bertrand, O., Berthoz, A., Kahane, P., et al. (2009). Task-related gamma-band dynamics from an intracerebral perspective: review and implications for surface EEG and MEG. Hum. Brain Mapp. *30*, 1758–1771.

Jokisch, D., and Jensen, O. (2007). Modulation of gamma and alpha activity during a working memory task engaging the dorsal or ventral stream. J. Neurosci. Off. J. Soc. Neurosci. *27*, 3244–3251.

de Jong, B.M. (2011). Neurology of widely embedded free will. Cortex J. Devoted Study Nerv. Syst. Behav. *47*, 1160–1165.

Kable, J.W., and Glimcher, P.W. (2009). The Neurobiology of Decision: Consensus and Controversy. Neuron *63*, 733–745.

Kagan, I., Iyer, A., Lindner, A., and Andersen, R.A. (2010). Space representation for eye movements is more contralateral in monkeys than in humans. Proc. Natl. Acad. Sci. *107*, 7933–7938.

Kayser, C., Kim, M., Ugurbil, K., Kim, D.-S., and König, P. (2004). A comparison of hemodynamic and neural responses in cat visual cortex using complex stimuli. Cereb. Cortex N. Y. N 1991 *14*, 881–891.

Khonsari, R.H., Lobel, E., Milea, D., Lehéricy, S., Pierrot-Deseilligny, C., and Berthoz, A. (2007). Lateralized parietal activity during decision and preparation of saccades. Neuroreport *18*, 1797–1800.

Kim, J.N., and Shadlen, M.N. (1999). Neural correlates of a decision in the dorsolateral prefrontal cortex of the macaque. Nat. Neurosci. *2*, 176–185.

Kucewicz, M.T., Berry, B.M., Kremen, V., Brinkmann, B.H., Sperling, M.R., Jobst, B.C., Gross, R.E., Lega, B., Sheth, S.A., Stein, J.M., et al. (2017). Dissecting gamma frequency activity during human memory processing. Brain J. Neurol. *140*, 1337–1350.

Lachaux, J.P., Rudrauf, D., and Kahane, P. (2003). Intracranial EEG and human brain mapping. J. Physiol. Paris *97*, 613–628.

Lachaux, J.-P., Hoffmann, D., Minotti, L., Berthoz, A., and Kahane, P. (2006a). Intracerebral dynamics of saccade generation in the human frontal eye field and supplementary eye field. NeuroImage *30*, 1302–1312.

Lachaux, J.-P., Hoffmann, D., Minotti, L., Berthoz, A., and Kahane, P. (2006b). Intracerebral dynamics of saccade generation in the human frontal eye field and supplementary eye field. NeuroImage *30*, 1302–1312.

Lachaux, J.-P., Fonlupt, P., Kahane, P., Minotti, L., Hoffmann, D., Bertrand, O., and Baciu, M. (2007). Relationship between task-related gamma oscillations and BOLD signal: New insights from combined fMRI and intracranial EEG. Hum. Brain Mapp. *28*, 1368–1375.

Lachaux, J.-P., Axmacher, N., Mormann, F., Halgren, E., and Crone, N.E. (2012). High-frequency neural activity and human cognition: past, present and possible future of intracranial EEG research. Prog. Neurobiol. *98*, 279–301.

Lemm, S., Blankertz, B., Dickhaus, T., and Müller, K.-R. (2011). Introduction to machine learning for brain imaging. NeuroImage *56*, 387–399.

Leszczynski, M., and Schroeder, C.E. (2019). The Role of Neuronal Oscillations in Visual Active Sensing. Front. Integr. Neurosci. *13*.

Logothetis, N.K., Pauls, J., Augath, M., Trinath, T., and Oeltermann, A. (2001). Neurophysiological investigation of the basis of the fMRI signal. Nature *412*, 150–157.

Manning, J.R., Jacobs, J., Fried, I., and Kahana, M.J. (2009). Broadband shifts in local field potential power spectra are correlated with single-neuron spiking in humans. J. Neurosci. Off. J. Soc. Neurosci. *29*, 13613–13620.

McDowell, J.E., Dyckman, K.A., Austin, B.P., and Clementz, B.A. (2008). Neurophysiology and neuroanatomy of reflexive and volitional saccades: evidence from studies of humans. Brain Cogn. *68*, 255–270.

Medendorp, W.P., Goltz, H.C., and Vilis, T. (2006). Directional selectivity of BOLD activity in human posterior parietal cortex for memory-guided double-step saccades. J. Neurophysiol. *95*, 1645–1655.

Milea, D., Lobel, E., Lehéricy, S., Leboucher, P., Pochon, J.-B., Pierrot-Deseilligny, C., and Berthoz, A. (2007). Prefrontal cortex is involved in internal decision of forthcoming saccades. Neuroreport *18*, 1221–1224.

Mitzdorf, U. (1985). Current source-density method and application in cat cerebral cortex: investigation of evoked potentials and EEG phenomena. Physiol. Rev. *65*, 37–100.

Moon, S.Y., Barton, J.J.S., Mikulski, S., Polli, F.E., Cain, M.S., Vangel, M., Hämäläinen, M.S., and Manoach, D.S. (2007). Where left becomes right: a magnetoencephalographic study of sensorimotor transformation for antisaccades. NeuroImage *36*, 1313–1323.

Mukamel, R., Gelbard, H., Arieli, A., Hasson, U., Fried, I., and Malach, R. (2005). Coupling between neuronal firing, field potentials, and FMRI in human auditory cortex. Science *309*, 951–954.

Murthy, V.N., and Fetz, E.E. (1992). Coherent 25- to 35-Hz oscillations in the sensorimotor cortex of awake behaving monkeys. Proc. Natl. Acad. Sci. *89*, 5670–5674.

Niessing, J., Ebisch, B., Schmidt, K.E., Niessing, M., Singer, W., and Galuske, R.A.W. (2005). Hemodynamic signals correlate tightly with synchronized gamma oscillations. Science *309*, 948–951.

Nir, Y., Fisch, L., Mukamel, R., Gelbard-Sagiv, H., Arieli, A., Fried, I., and Malach, R. (2007). Coupling between neuronal firing rate, gamma LFP, and BOLD fMRI is related to interneuronal correlations. Curr. Biol. CB *17*, 1275–1285.

Ojemann, G.A., Ramsey, N.F., and Ojemann, J. (2013). Relation between functional magnetic resonance imaging (fMRI) and single neuron, local field potential (LFP) and electrocorticography (ECoG) activity in human cortex. Front. Hum. Neurosci. *7*.

Oliveira, F.T.P., Diedrichsen, J., Verstynen, T., Duque, J., and Ivry, R.B. (2010). Transcranial magnetic stimulation of posterior parietal cortex affects decisions of hand choice. Proc. Natl. Acad. Sci. *107*, 17751–17756.

Olk, B., Chang, E., Kingstone, A., and Ro, T. (2006). Modulation of antisaccades by transcranial magnetic stimulation of the human frontal eye field. Cereb. Cortex N. Y. N 1991 *16*, 76–82.

Ossandón, T., Jerbi, K., Vidal, J.R., Bayle, D.J., Henaff, M.-A., Jung, J., Minotti, L., Bertrand, O., Kahane, P., and Lachaux, J.-P. (2011). Transient Suppression of Broadband Gamma Power in the Default-Mode Network Is Correlated with Task Complexity and Subject Performance. J. Neurosci. *31*, 14521–14530.

Ossandón, T., Vidal, J.R., Ciumas, C., Jerbi, K., Hamamé, C.M., Dalal, S.S., Bertrand, O., Minotti, L., Kahane, P., and Lachaux, J.-P. (2012). Efficient "pop-out" visual search elicits sustained broadband γ activity in the dorsal attention network. J. Neurosci. Off. J. Soc. Neurosci. *32*, 3414–3421.

Park, C., Plank, M., Snider, J., Kim, S., Huang, H.C., Gepshtein, S., Coleman, T.P., and Poizner, H. (2014). EEG gamma band oscillations differentiate the planning of spatially directed movements of the arm versus eye: multivariate empirical mode decomposition analysis. IEEE Trans. Neural Syst. Rehabil. Eng. Publ. IEEE Eng. Med. Biol. Soc. *22*, 1083–1096.

Pastor-Bernier, A., and Cisek, P. (2011). Neural correlates of biased competition in premotor cortex. J. Neurosci. Off. J. Soc. Neurosci. *31*, 7083–7088.

Pastor-Bernier, A., Tremblay, E., and Cisek, P. (2012). Dorsal premotor cortex is involved in switching motor plans. Front. Neuroengineering *5*.

Pedregosa, F., Varoquaux, G., Gramfort, A., Michel, V., Thirion, B., Grisel, O., Blondel, M., Müller, A., Nothman, J., Louppe, G., et al. (2012). Scikit-learn: Machine Learning in Python.

Pesaran, B., Pezaris, J.S., Sahani, M., Mitra, P.P., and Andersen, R.A. (2002). Temporal structure in neuronal activity during working memory in macaque parietal cortex. Nat. Neurosci. *5*, 805–811.

Pesaran, B., Nelson, M.J., and Andersen, R.A. (2008). Free choice activates a decision circuit between frontal and parietal cortex. Nature *453*, 406–409.

Petit, L., Clark, V.P., Ingeholm, J., and Haxby, J.V. (1997). Dissociation of saccade-related and pursuit-related activation in human frontal eye fields as revealed by fMRI. J. Neurophysiol. *77*, 3386–3390.

Pfurtscheller, G., and Lopes da Silva, F.H. (1999). Event-related EEG/MEG synchronization and desynchronization: basic principles. Clin. Neurophysiol. Off. J. Int. Fed. Clin. Neurophysiol. *110*, 1842–1857.

Pfurtscheller, G., Stancák, A., and Neuper, C. (1996). Post-movement beta synchronization. A correlate of an idling motor area? Electroencephalogr. Clin. Neurophysiol. *98*, 281–293.

Pierrot-Deseilligny, C., Ploner, C.J., Muri, R.M., Gaymard, B., and Rivaud-Pechoux, S. (2002). Effects of cortical lesions on saccadic: eye movements in humans. Ann. N. Y. Acad. Sci. *956*, 216–229.

Platt, M.L., and Glimcher, P.W. (1999). Neural correlates of decision variables in parietal cortex. Nature *400*, 233–238.

Rainer, G., Rao, S.C., and Miller, E.K. (1999). Prospective coding for objects in primate prefrontal cortex. J. Neurosci. Off. J. Soc. Neurosci. *19*, 5493–5505.

Raschka, S. (2018). Model Evaluation, Model Selection, and Algorithm Selection in Machine Learning.

Ray, S., and Maunsell, J.H.R. (2011). Different Origins of Gamma Rhythm and High-Gamma Activity in Macaque Visual Cortex. PLOS Biol. *9*, e1000610.

Ray, S., Crone, N.E., Niebur, E., Franaszczuk, P.J., and Hsiao, S.S. (2008). Neural Correlates of High-Gamma Oscillations (60–200 Hz) in Macaque Local Field Potentials and Their Potential Implications in Electrocorticography. J. Neurosci. *28*, 11526–11536.

Resulaj, A., Kiani, R., Wolpert, D.M., and Shadlen, M.N. (2009). Changes of mind in decision-making. Nature *461*, 263–266.

Riley, M.R., and Constantinidis, C. (2015). Role of Prefrontal Persistent Activity in Working Memory. Front. Syst. Neurosci. *9*, 181.

Romo, R., and de Lafuente, V. (2013). Conversion of sensory signals into perceptual decisions. Prog. Neurobiol. *103*, 41–75.

Roux, F., Wibral, M., Mohr, H.M., Singer, W., and Uhlhaas, P.J. (2012). Gamma-Band Activity in Human Prefrontal Cortex Codes for the Number of Relevant Items Maintained in Working Memory. J. Neurosci. *32*, 12411–12420.

Rushworth, M.F.S., Johansen-Berg, H., Göbel, S.M., and Devlin, J.T. (2003). The left parietal and premotor cortices: motor attention and selection. NeuroImage *20 Suppl 1*, S89-100.

Sakamoto, A., Lüders, H., and Burgess, R. (1991). Intracranial recordings of movement-related potentials to voluntary saccades. J. Clin. Neurophysiol. Off. Publ. Am. Electroencephalogr. Soc. *8*, 223–233.

Sanes, J.N., and Donoghue, J.P. (1993). Oscillations in local field potentials of the primate motor cortex during voluntary movement. Proc. Natl. Acad. Sci. U. S. A. *90*, 4470–4474.

Schall, J.D., and Bichot, N.P. (1998). Neural correlates of visual and motor decision processes. Curr. Opin. Neurobiol. *8*, 211–217.

Sendhilnathan, N., Basu, D., and Murthy, A. (2017). Simultaneous analysis of the LFP and spiking activity reveals essential components of a visuomotor transformation in the frontal eye field. Proc. Natl. Acad. Sci. *114*, 6370–6375.

Shadlen, M.N., and Newsome, W.T. (2001). Neural basis of a perceptual decision in the parietal cortex (area LIP) of the rhesus monkey. J. Neurophysiol. *86*, 1916–1936.

Siegel, M., Buschman, T.J., and Miller, E.K. (2015). Cortical information flow during flexible sensorimotor decisions. Science *348*, 1352–1355.

Soon, C.S., Brass, M., Heinze, H.-J., and Haynes, J.-D. (2008). Unconscious determinants of free decisions in the human brain. Nat. Neurosci. *11*, 543–545.

Stokes, M.G. (2015). "Activity-silent" working memory in prefrontal cortex: a dynamic coding framework. Trends Cogn. Sci. *19*, 394–405.

Sugrue, L.P., Corrado, G.S., and Newsome, W.T. (2004). Matching behavior and the representation of value in the parietal cortex. Science *304*, 1782–1787.

Sweeney, J.A., Luna, B., Keedy, S.K., McDowell, J.E., and Clementz, B.A. (2007). fMRI Studies of Eye Movement Control: Investigating the Interaction of Cognitive and Sensorimotor Brain Systems. NeuroImage *36*, T54–T60.

Talairach, J., and Tournoux, P. (1988). Co-Planar Stereotaxic Atlas of the Human Brain: 3-D Dimensional Proportional System: An Approach to Cerebral Imaging (Stuttgart: Thieme-Stratton Corp).

Tallon-Baudry, C., Bertrand, O., Peronnet, F., and Pernier, J. (1998). Induced gamma-band activity during the delay of a visual short-term memory task in humans. J. Neurosci. Off. J. Soc. Neurosci. *18*, 4244–4254.

Tobler, P.N., and Müri, R.M. (2002). Role of human frontal and supplementary eye fields in double step saccades. NeuroReport *13*, 253.

Van Der Werf, J., Buchholz, V.N., Jensen, O., and Medendorp, W.P. (2009). Neuronal synchronization in human parietal cortex during saccade planning. Behav. Brain Res. *205*, 329–335.

Werf, J.V.D., Jensen, O., Fries, P., and Medendorp, W.P. (2008). Gamma-Band Activity in Human Posterior Parietal Cortex Encodes the Motor Goal during Delayed Prosaccades and Antisaccades. J. Neurosci. *28*, 8397–8405.

Werf, J.V.D., Jensen, O., Fries, P., and Medendorp, W.P. (2010). Neuronal Synchronization in Human Posterior Parietal Cortex during Reach Planning. J. Neurosci. *30*, 1402–1412.

Whittingstall, K., and Logothetis, N.K. (2009). Frequency-band coupling in surface EEG reflects spiking activity in monkey visual cortex. Neuron *64*, 281–289.

Yamamoto, J., Ikeda, A., Satow, T., Matsuhashi, M., Baba, K., Yamane, F., Miyamoto, S., Mihara, T., Hori, T., Taki, W., et al. (2004). Human eye fields in the frontal lobe as studied by epicortical recording of movement-related cortical potentials. Brain J. Neurol. *127*, 873–887.

Yang, T., and Shadlen, M.N. (2007). Probabilistic reasoning by neurons. Nature *447*, 1075–1080.